HHS Public Access

Author manuscript

World Neurosurg. Author manuscript; available in PMC 2018 February 20.

Published in final edited form as:

World Neurosurg. 2017 July ; 103: 600–610. doi:10.1016/j.wneu.2017.03.088.

First Application of 7T Magnetic Resonance Imaging in Endoscopic Endonasal Surgery of Skull Base Tumors

Thomas F Barrett, BA[a,*], **Hadrien A Dyvorne, PhD**[b], **Francesco Padormo, PhD**[b], **Puneet S Pawha, MD**[c], **Bradley N Delman, MD**[c], **Raj K Shrivastava, MD**[a], and **Priti Balchandani, PhD**[b]

[a]Mount Sinai Medical Center, Department of Neurosurgery, One Gustave L. Levy Place, New York, NY, USA 10029

[b]Mount Sinai Medical Center, The Translational and Molecular Imaging Institute, 1470 Madison Avenue, Floor 1, New York, NY, USA 10029

[c]Mount Sinai Medical Center, Department of Radiology, One Gustave L. Levy Place, Box 1234, New York, NY, USA 10029

Abstract

Background—Successful endoscopic endonasal surgery for the resection of skull base tumors is reliant on preoperative imaging to delineate pathology from the surrounding anatomy. The increased signal-to-noise ratio afforded by 7T MRI can be used to increase spatial and contrast resolution, which may lend itself to improved imaging of skull base. In this study, we apply a 7T imaging protocol to patients with skull base tumors and compare the images to clinical standard of care.

Methods—Images were acquired at 7T on 11 patients with skull base lesions. Two neuroradiologists evaluated clinical 1.5T, 3T, and 7T scans for detection of intracavernous cranial nerves and ICA branches. Detection rates were compared. Images were utilized for surgical planning and uploaded to a neuronavigation platform and used to guide surgery.

Results—Image analysis yielded improved detection rates of cranial nerves and ICA branches at 7T. 7T images were successfully incorporated into preoperative planning and intraoperative neuronavigation.

Conclusion—Our study represents the first application of 7T MRI to the full neurosurgical workflow for endoscopic endonasal surgery. We detected higher rates of cranial nerves and ICA branches at 7T MRI compared to 3T and 1.5 T, and found that integration of 7T into surgical planning and guidance was feasible. These results suggest a potential for 7T MRI to reduce surgical complications. Future studies comparing standardized 7T, 3T, and 1.5 T MRI protocols in a larger number of patients are warranted to determine the relative benefit of 7T MRI for endonasal endoscopic surgical efficacy.

Keywords

7T MRI; Ultrahighfield MRI; Endoscopic Endonasal Surgery; Skull base tumors

[*]Corresponding Author: Thomas.barrett@icahn.mssm.edu.

1. Introduction

Pituitary adenomas, craniopharyngiomas, meningiomas and other tumors affecting the skull base represent approximately 28% of all intracranial tumors[17,33] Due to the anatomic complexity of the skull base and the involvement by these tumors of nearby cranial nerves, optic structures, and portions of the internal carotid artery (ICA), these tumors post some of the most complex challenges in neurosurgery. Endoscopic endonasal surgery (EES), has emerged as an effective approach for the resection of pituitary adenomas,[7,13] craniopharyngiomas,[15,20] suprasellar meningioma,[25,27] chordomas,[14] and chondrosarcomas.[32] While the endoscope provides a wide-angle, high-definition view of the surgical field, [9] this surgical modality is greatly augmented by the use of intraoperative neuronavigation platforms. These systems create maps from preoperative magnetic resonance imaging (MRI) and computed tomography (CT) imaging and allow the real-time tracking of surgical instruments' position during surgery, thereby allowing the surgeon to see what lies beyond the view of the endoscope. Together, the endoscope and navigation platform allow the surgeon better visualization of tumor boundaries[24,31], tumor composition[1,36], and the tumor's relationship to nearby cranial nerves and branches of the ICA[21]. Injury to these neural and vascular structures leads to significant patient morbidity, and possibly mortality[16]. Therefore, high quality preoperative MRI is necessary to minimize patient harm and to guide surgery with the highest efficacy.

Recently, MR scanners with a static magnetic field (B_0) of 7T have been used to image brain anatomy and pathology *in vivo*, with exquisite and unprecedented detail.[26] The primary benefit of 7T imaging is the substantial increase in the signal-to-noise ratio (SNR), which increases supralinearly with the strength of B_0.[38] This higher SNR confers the ability to acquire images at higher resolution than lower field strengths, improving visualization of microanatomy,[26] and cranial nerves.[18,19] Longer T_1 values, coupled with higher SNR, also result in improved time-of-flight magnetic resonance angiography (TOF MRA), which allows for detectability of vessels as small as third-order ICA branches with better image quality than 3T MRI.[23,44] As a procedure that relies heavily on imaging for planning and intraoperative navigation, it follows logically that EES would benefit from the particularly effective elucidation of the delicate vasculature and cranial nerves adjacent to and involved with skull base tumors possible at 7T.

To date, studies of brain tumors with 7T MRI have been limited in number, skull base lesions have been infrequently investigated.[3] Accurately imaging the skull base at 7T can be technically challenging due to the increased field inhomogeneity seen with increasing B_0 and artifacts resulting from the amplified susceptibility effects of the bone-air interfaces in the paranasal and sphenoid sinuses.[35,41] Two studies by *De Rotte et al.* have demonstrated the feasibility of imaging the pituitary gland as well as improved detection of clinically suspected microadenomas at 7T MRI.[12-11] While these studies were the first to demonstrate the feasibility of imaging the pituitary gland and microadenomas at 7T, they did not include 3T images for comparison nor did they include analysis of the surrounding neural and vascular structures of most concern for surgical approaches to the sellar and parasellar spaces.

In this study, we utilized 7T MRI sequences to accurately image the skull base and assessed the feasibility of integrating this advanced imaging at 7T into neurosurgical flow in a series of patients presenting with skull base pathology who were candidates for EES. We report our experience in the first 11 patients imaged, planned, and operated upon using 7T MRI and surgical navigation. We perform a detailed analysis of image quality, rate visibility of neural and vascular structures involved by sellar and parasellar tumors, and report feasibility of integration into neurosurgical planning and intraoperative guidance.

2. Material and Methods

2.1. Patients

The institutional review board (IRB) of the Mount Sinai Medical Center approved 7T MRI imaging for clinical research purposes. All patients had diagnostic MRI studies completed at clinical field strengths (1.5T or 3T) and CT (images acquired with 1mm slice thickness using standard stereotactic protocol), which were used throughout their treatment to ensure they received clinical standard of care. All patients provided informed consent before each scan. Between September 2014 and October 2015, 11 patients with sellar lesions underwent 7T MRI. Of these 11 patients, two had a 3T scan performed according to our research protocol. EES for tumor resection was performed with the use of an intraoperative neuronavigational platform (BrainLab ENT Navigation, BrainLab AG, Feldkirchen, Germany).

2.2. MRI hardware and sequences

All 7T scans were conducted using a whole-body scanner (Magnetom, Siemens, Erlangen, Germany) and a 1-channel transmit and 32-channel receive head coil (Nova Medical, Siemens, Erlangen, Germany). Our objective was to obtain full anatomical coverage of and optimal B_0 field homogeneity within the skull base region containing the tumor. 7T MR images for this study were acquired using three sequences: 3D T1-weighted (T1W) magnetization-prepared rapid gradient echo (MP2-RAGE)[30], a T2-weighted turbo spine echo (T2W-TSE) and TOF MRA. The prescribed region of interest for specific absorption rate (SAR) limited sequences with reduced spatial coverage, such as TSE, was centered to encompass the tumor and skull base structures. B0 shimming was performed using the standard scanner software, with the shim volume placed over the skull base region of interest. Radiofrequency (RF) pulse amplitudes were set to be 10% higher than the optimum value calculated for the center of the brain, in order to overcome the reduced transmit field amplitude in the skull base. Specific sequence parameters can be found in Tables 1 and 2. Clinical diagnostic scans were acquired with 1.5 T MR scanners from outpatient clinical settings. Additionally, a subset of patients received an additional 3T MRI (Skyra, Siemens, Erlangen, Germany) according to our research protocol, which included the same sequences as the 7T scans. TOF MRA images were assessed for utility in surgical planning, but were not used in our comparative image quality analysis because a TOF MRA sequence was not included in most of the 1.5 T MR studies.

2.3. Intraoperative Neuronavigation and Surgical Approach

Images acquired at 1.5T or 3T were uploaded to an intraoperative neuronavigation platform, with the addition of MP2-RAGE, T2-weighted TSE, and TOF MRA sequences acquired at 7T. Images from 3T or 1.5 T studies were utilized for guidance, with 7T images simultaneously utilized by the neurosurgeon (RS).

CT and 7T MR images were fused to create complex navigational sequences that were registered to each patient's superficial facial anatomy. In order to register the location of the endoscope on displayed images, infrared fiducial markers were used in conjunction with a mounted infrared camera and a receiver on a headband. All surgeries were performed by the same neurosurgeon (RS).

2.4. Image Analysis

Non-contrast enhanced T1W and T2W images from 7T, 3T, and 1.5T MR scans were reviewed independently by two radiologists (BD and PP) with 16 years and 10 years of experience in neuroradiology, respectively. They rated their ability to visualize anatomical structures or tumor features, listed in detail below, on a 0–2 scale (0 = definitely not visible, 1 = maybe visible, 2 = definitely visible). All instances of discrepant ratings were resolved by consensus between the two radiologists. Definitions of these scores are given below in reference to the structure to which they apply.

2.4.1. Cranial Nerves—The ability to delineate cranial nerves (CN) II, III, IV, V1, V2, and VI within the plane of the tumor was assessed. The cranial nerves were defined as hypointense spots on coronal sections of T_2-weighted images. For CN II, a score of 2 was given if the optic nerve could be traced to the chiasm and to the optic tract. A score of 1 was given if this pathway was obscured in any image slices. A score of 0 was given if this pathway could not be delineated. For CNs III, IV, V1, V2, and VI, a score of 2 was given when the nerves could be followed from their respective exit points at the brain stem through the cavernous sinus. A score of 1 was given when the nerve's course was obscured but could be inferred from preceding images in the series. A score of 0 was given when the nerve could not be differentiated from the surrounding anatomy in the cavernous sinus. For those patients with scans at multiple field strengths, rates of detection of each nerve were compared.

2.4.2. Branches of the ICA—We attempted visualization of major branches of the ICA whose locations are particularly relevant for endonasal skull base approaches, namely the anterior cerebral artery (ACA), the middle cerebral artery (MCA), the superior hypophyseal artery (SH), the posterior communicating artery (PCommA), the ophthalmic artery (O) and the anterior choroidal artery (AChA). A score of 2 was given to any vessel that could be traced back to its parent vessel. A score of 1 was given to any vessel whose path to its parent vessel was implied but not clearly visualized. A score of 0 was given if the vessel could not be seen. For those patients with scans at multiple field strengths, rates of detection of each ICA branch were compared.

2.4.3. Tumor Characteristics—Aspects of the tumor (such as presence of a cystic/hemorrhagic, and visibility of neovasculature within the tumor) and its relation to adjacent anatomy (i.e., optic chiasm compression) were graded. A cystic component was defined as a locus within the lesion that was hypointense on T_1-weighted images and hyperintense on T_2-weighted images. A hemorrhagic component was defined as a locus that was hyperintense on both T_1- and T_2-weighted images. Tumor neovasculature was considered visible vessels within the lesion that were distinct from anatomically normal vessels. The optic chiasm was considered compressed if lesion growth extended superiorly, abutted the nerves, and altered their normal course.

2.4.4. Image artifacts—Two MR physicists (PB and HD) rated images on a 5-point Likert scale (1 = negligible artifacts, 2 = minimal artifacts, 3 = moderate artifacts, 4 = high artifacts, and 5 = severe artifacts), coming to a consensus to assess three major sources of image artifact: motion, B_0 field inhomogeneity, and B_1 signal/contrast loss from images obtained at 7T, 3T and 1.5T.

3. Results

3.1. Patients, Surgery, and Pathology

Eleven patients (4M and 7F; average age = 48, range = 31–64) with suspected sellar pathology were scanned using 7T MRI. For image guidance, 9 of these patients had an outside clinical scan performed prior to surgery and the other two had a 3T scanned performed at our institution. Of these patients, 9 underwent primary EES with neuronavigation for attempted resection of their skull base pathology. Two patients underwent craniotomy, one with a right orbitocranial approach[40] and the other with a left preauricular frontal approach[39]. Of the 9 primary EES cases, one patient with an exceptionally large pituitary macroadenoma underwent a second open procedure (right orbitofrontal craniotomy[40]).

Histopathological analysis revealed that there were 8 pituitary adenomas (3 null types, 2 gondatroph types, 1 somatotroph type, and 2 in which a subclassification was not made). Additionally, there was a meningioma (WHO Grade 1), and adamantinomatous craniopharyngioma, and one sample in which no pathology was seen.

3.2. Image Analysis

Eight patients' images were available for comparison (7 patients with only high-resolution skull base sequences at 1.5T, one with only 7T and 3T images, and one with all three). In the patient with both 3T and 1.5T available for comparison, 3T images were used. Two patients were excluded because their clinical scans were not appropriate (one low-resolution whole-brain scan; one brain CT). One patient was excluded due to prior surgery in the ROI.

Figure 1 juxtaposes rates of visualization of each cranial nerve and ICA branch as detected by 7T, 3T, and 1.5T in the 8 patients whose images could be compared. There were no instances in which a structure seen at 3T was not seen at 7T. Conversely, there were 7 structures definitely seen and 4 maybe seen at 7T that were not seen at 3T. Detection of the

smaller nerves and vessels was higher at 7T compared to 1.5T and 3T. Large vessel and cranial nerve II detection rates were comparable at all field strengths.

Figures 2, 3, 4, 5, and 6 are images from patients for whom we were able to acquire both 3T and 7T images. They illustrate better nerve-tumor delineation, tumor-gland delineation, the medial cavernous sinus wall, and increased vessel conspicuity at 7T MRI. Table 3 summarizes the tumor characteristics observed at each field strength. Figure 7 shows a giant adenoma at 7T with surrounding vessels and vascularity within the tumor highlighted. Table 4 displays rates of image artifacts at each field strength as rated by the two MR physicists.

4. Discussion

With our initial 11 subjects, we demonstrated the feasibility of acquiring images of the sellar and parasellar regions at 7T MRI and the use of these images at every stage of the neurosurgical workflow, including use intraoperatively for neuronavigation. Furthermore, we saw increased rates of visualization of cranial nerves and ICA branches using 7T MRI compared to 1.5T and 3T imaging (Figure 1). Motion, B_0, and B_1 artifacts were seen at higher rates at 7T than both 1.5T and 3T, though these artifacts were not severe enough in any instance to affect the clinical utility of 7T images. The remainder of this section will place our findings in the context of past and present work, will discuss limitations of our study, and will offer suggestions for future work.

4.1. Cranial Nerves in the Cavernous Sinus

To date, there have been few studies investigating the use of 7T MRI for visualization of the cranial nerves. In a series of three healthy subjects, Grams et al. demonstrated excellent visualization of all cranial nerves exiting the brain stem with a variety of 7T sequences, most notably with the true fast imaging in steady state precession (TrueFISP) sequence.[19] In a later series of healthy subjects (six scanned at 7T, two of which were additionally scanned at 3T), Gizewski et al. demonstrated excellent visualization of brain stem structures and exiting nerves at 7T, including structures that were not detectable at 3T, such as the vagal and glossopharyngeal nerves.[18] While de *Rotte et al.* successfully demonstrated imaging of the pituitary gland and chemically confirmed microadenomas with 7T images,[10,12] their studies did not analyze the surrounding cavernous anatomy. To the best of the authors' knowledge, no previous studies have demonstrated the visualization of the cranial nerves with 7T MRI as they course through the cavernous sinus in neither healthy subjects nor in patients with local pathology.

In our analysis of cranial nerve detection, all three field strengths had comparable detection of the larger nerves (CN II, and CN V1,2). Notable differences were seen in the detection of the smaller three nerves (CN III, IV, and VI), particularly when comparing T2W TSE sequences at 7T to 1.5 T MRI. While we had only two patients scanned at both 3T and 7T, improvements in tumor-nerve delineation with 7T MRI can be appreciated qualitatively by juxtaposing images from the same patient acquired at both field strengths (Figure 5). The increased SNR provided by 7T can be used to increase both spatial resolution as well as contrast resolution, which is demonstrated nicely in Figure 6. Improved localization of these cranial nerves with 7T MRI may help to optimize the planned surgical approach (i.e.,

endoscopically versus transcranially) as well as minimize iatrogenic injuries to these structures.

Our present study did not include any contrast-enhanced sequences. The cavernous sinus enhances significantly after the administration of a contrast agent, and the cranial nerves can be visualized as regions of hypointensity within these rapidly enhancing venous portions on both 1.5T and 3T scanners.[2,28,37,45–47] In a comparison of 3T MRI versus 1.5T and 1T MRI in 21 patients with sellar and parasellar pathologies, *Wolfsberger et al.* compared the fraction of nerves depicted per cavernous sinus side (i.e., maximum of five nerves in each lateral sinus) using contrast-enhanced (CE) T1-weighted sequences. With 3T MRI they found an average of four nerves in each cavernous sinus compared to an average of three at 1.5T or 1T ($p<0.001$), the most notable differences being with the fourth and sixth nerves, seen in 67% and 26% of cases, respectively.[45] Future work should focus on optimizing 7T contrast-enhanced sequences for skull base imaging, and comparing the utility of these sequences to 3T and 1.5T images.

Additionally, high-resolution 3D steady-state free precession (SSFP) sequences allow for detailed and accurate assessment of both normal anatomy and pathology involving the skull base and allow for localization of structural causes of cranial nerve palsies.[5] In particular, CE-3D constructive interference in steady state (CISS) and fast imaging employing steady-state acquisition (FIESTA) have both demonstrated excellent delineation of the cavernous cranial nerve segments in healthy subjects.[2,47] Neoplastic involvement of the cavernous sinus, however, may diminish contrast enhancement and thereby less accurate detection of the intracavernous nerve segments.[2,46] T1W sequences, such as MPRAGE and MRA, enhance more intensely than do SSFP sequences.[28] *Linn et al.* demonstrated that this increased sinus enhancement with CE MRA led to excellent intracavernous nerve detection in both healthy subjects and patients with pituitary adenomas.[28]

Due to the exceptional sensitivity of SSFP imaging to B_0 inhomogeneity, we excluded such a sequence from our current protocol. Some sequences, such as balanced SSFP, have been successfully utilized to image multiple brain regions including the hippocampus, basal cisterns, and the deep brain nuclei at 7T, though long scanning times remain an obstacle.[48] Future work from our group and others will involve sequence development and improved shimming to create an SSFP sequence that will counteract the increased inhomogeneity and will facilitate further improvements in high resolution skull base imaging.[34]

4.2 Branches of the ICA

Damage to the ICA during EES is a rare but feared complication of EES that can result in cranial nerve palsies, stroke, and death. New postoperative visual defects resulting as complications of EES occur in 2.3% to 4.8% of cases.[22,29] Vascular injury is less common (0.24%), but when it occurs it is catastrophic and often lethal.[43] Reported rates of carotid injury range from 0.3% (in pituitary adenomas) to 2% (in chordomas and chondrosarcomas).[16] Therefore, preoperative knowledge of a tumor's relationship to the ICA and its branches is crucial to maximize resection while minimizing the risk of catastrophic bleeding.

In our comparison analysis of T2W TSE images acquired at 7T to comparable images at 3T and 1.5 T MRI, we noted overall higher rates of visualization of the ICA branches as flow voids with the 7T MRI (Figure 1). This difference was most notable in the detection of smaller caliber vessels, namely O, PCOM and AChA (the SH was not detected at any field strength in any subject). Additionally, small perforating vessels can be appreciated branching from the large caliber cerebral vessels due to the improved spatial resolution achieved with these 7T images (Figure 5). Additionally, we acquired TOF MRA in our two patients with both 7T and 3T imaging. While these images were not involved in our quantitative assessment of visible vessels, smaller arteries feeding the tumor and parenchyma can be appreciated at 7T than were achievable with 3T images in the same patient (Figure 3). Improved vessel detection may help reduce vascular complications, and it may improve management of non-tumor pathologies, such as cerebral aneurysms.[4,42]

4.3 Tumor Characteristics

Tumor characteristics such as size, firmness, invasion of cavernous sinus, and degree of neovascularity are important factors that can significantly impact surgical time, technical difficulty, and extent of resection in sellar and parasellar masses.[6,22,31] In pituitary adenomas, in particular, MRI allows for both prediction of extent of invasion as well as delineation of tumor from healthy gland.[8,24] The increased spatial and contrast resolution afforded by 7T imaging may allow for more accurate prediction of cavernous sinus invasion, as seen in Figure 6A.

In our patients with imaging studies available at multiple field strengths, tumor characteristics were all seen at similar rates with the exception of tumor neovascularity (Table 3), which was seen exceptionally well with 7T MRI. Figure 7 shows a particularly striking example of this tumor vasculature in the context of a patient with a giant pituitary adenoma. Preoperative knowledge of a tumor with such high vascularity will allow the surgeon to anticipate bleeding.

4.4 Limitations

Known limitations of 7T MRI include increased field inhomogeneity causing signal loss and artifacts as well as higher sensitivity to motion for very high resolution scans. Therefore we performed a systematic analysis of these artifacts. Although motion, B_0, and B_1 artifacts were seen more frequently at 7T compared to 1.5T or 3T (Table 4), these artifacts did not interfere with the ROI in the surgical window. B_1 effects were seen frequently, but most reduced visualization of the temporal lobe and did not reduce visualization of the sellar and parasellar spaces. Susceptibility-artifacts due to bone-air interface, which have historically been problematic with 7T imaging, did not affect surgical planning.

The central limitation to our study is that our sample size was small and featured heterogeneous pathology. With such a sample, we were not able make statistical comparisons. Additionally, 1.5T and 3T MRI are both currently considered to be standard-of-care for the planning and intraoperative navigation of EES. Some studies have demonstrated an improved detection rate of intracavernous cranial nerves and CS invasion with 3T MRI compared to 1T and 1.5T.[37,45] In future work, larger sample sizes with patients

receiving standardized MRI studies at multiple field strengths will be needed to compare the relative clinical utility of 7T MRI compared to current clinical standards.

Nevertheless, these preliminary results are promising and warrant further investigation comparing the utility of 7T MRI to both 3T and 1.5 T MRI for presurgical imaging of skull base anatomy and pathology. Future studies will ideally report sequence optimization for adequate skull base coverage with 7T MRI. They should include standardized imaging protocols for all three field strengths. They should also use more objective measures, such as comparison of surgical times and corroborating of surgical findings to findings predicted by MRI.

5. Conclusion

Our study represents the first successful application of 7T MRI to the preoperative workup and intraoperative neuronavigation of patients with skull base tumors. In our initial series of patients, we were able to detect higher rates of involved cranial nerves and ICA branches with 7T MRI compared to 3T and 1.5 T MRI. These results suggest a potential for high-resolution structural imaging and TOF MRA at 7T to optimize surgical planning and minimize injury to these often-involved neural and vascular structures. Future studies comparing standardized 7T, 3T, and 1.5 T MRI protocols in a larger number of patients are warranted to determine the relative benefit of 7T MRI for skull base surgery and ultimately its clinical effect on patient outcomes.

Acknowledgments

6. Funding

This work was supported by the National Institute of Health (NIH-NINDS R00 NS070821, NIH R01 CA202911); Icahn School of Medicine Capital Campaign, Translational and Molecular Imaging Institute; Department of Radiology; Icahn School of Medicine's Summer Student Investigator Award.

References

1. Alimohamadi M, Sanjari R, Mortazavi A, Shirani M, Moradi Tabriz H, Hadizadeh Kharazi H, et al. Predictive value of diffusion-weighted MRI for tumor consistency and resection rate of nonfunctional pituitary macroadenomas. Acta Neurochir (Wien). 2014; 156:2245–2252. discussion 2252. [PubMed: 25338532]
2. Amemiya S, Aoki S, Ohtomo K. Cranial nerve assessment in cavernous sinus tumors with contrast-enhanced 3D fast-imaging employing steady-state acquisition MR imaging. Neuroradiology. 2009; 51:467–470. [PubMed: 19238368]
3. Barrett TF, Sarkiss CA, Dyvorne HA, Lee J, Balchandani P, Shrivastava RK. Application of Ultrahigh Field Magnetic Resonance Imaging in the Treatment of Brain Tumors: A Meta-Analysis. World Neurosurg. 2016; 86:450–465. [PubMed: 26409071]
4. Blankena R, Kleinloog R, Verweij BH, van Ooij P, Ten Haken B, Luijten PR, et al. Thinner Regions of Intracranial Aneurysm Wall Correlate with Regions of Higher Wall Shear Stress: A 7T MRI Study. AJNR Am J Neuroradiol. 2016; 37:1310–1317. [PubMed: 26892986]
5. Blitz AM, Aygun N, Herzka DA, Ishii M, Gallia GL. High Resolution Three-Dimensional MR Imaging of the Skull Base: Compartments, Boundaries, and Critical Structures. Radiol Clin North Am. 2017; 55:17–30. [PubMed: 27890185]

6. Cao L, Chen H, Hong J, Ma M, Zhong Q, Wang S. Magnetic resonance imaging appearance of the medial wall of the cavernous sinus for the assessment of cavernous sinus invasion by pituitary adenomas. J Neuroradiol. 2013; 40:245–251. [PubMed: 23886874]
7. Ceylan S, Koc K, Anik I. Endoscopic endonasal transsphenoidal approach for pituitary adenomas invading the cavernous sinus. J Neurosurg. 2010; 112:99–107. [PubMed: 19480546]
8. Cho, Charles H., Barkhoudarian, Garni, Hsu, Liangge, Bi, Wenya Linda, Zamani, Amir A., Laws, Edward R. Magnetic resonance imaging validation of pituitary gland compression and distortion by typical sellar pathology. Journal of Neurosurgery. 2013; 119:1461–1466. [PubMed: 24032703]
9. de Divitiis E. Endoscopic transsphenoidal surgery: stone-in-the-pond effect. Neurosurgery. 2006; 59:512–520. discussion 512–520. [PubMed: 16955032]
10. de Rotte AA, Groenewegen A, Rutgers DR, Witkamp T, Zelissen PM, Meijer FJ, et al. High resolution pituitary gland MRI at 7.0 tesla: a clinical evaluation in Cushing's disease. Eur Radiol. 2015
11. de Rotte AA, Groenewegen A, Rutgers DR, Witkamp T, Zelissen PM, Meijer FJ, et al. High resolution pituitary gland MRI at 7.0 tesla: a clinical evaluation in Cushing's disease. Eur Radiol. 2016; 26:271–277. [PubMed: 25991481]
12. de Rotte AA, van der Kolk AG, Rutgers D, Zelissen PM, Visser F, Luijten PR, et al. Feasibility of high-resolution pituitary MRI at 7.0 tesla. Eur Radiol. 2014; 24:2005–2011. [PubMed: 24871334]
13. Di Maio S, Cavallo LM, Esposito F, Stagno V, Corriero OV, Cappabianca P. Extended endoscopic endonasal approach for selected pituitary adenomas: early experience. J Neurosurg. 2011; 114:345–353. [PubMed: 21054140]
14. Fraser JF, Nyquist GG, Moore N, Anand VK, Schwartz TH. Endoscopic endonasal transclival resection of chordomas: operative technique, clinical outcome, and review of the literature. J Neurosurg. 2010; 112:1061–1069. [PubMed: 19698043]
15. Gardner PA, Kassam AB, Snyderman CH, Carrau RL, Mintz AH, Grahovac S, et al. Outcomes following endoscopic, expanded endonasal resection of suprasellar craniopharyngiomas: a case series. J Neurosurg. 2008; 109:6–16. [PubMed: 18590427]
16. Gardner PA, Tormenti MJ, Pant H, Fernandez-Miranda JC, Snyderman CH, Horowitz MB. Carotid artery injury during endoscopic endonasal skull base surgery: incidence and outcomes. Neurosurgery. 2013; 73:ons261–269. discussion ons269–270. [PubMed: 23695646]
17. Ginsberg LE. Neoplastic diseases affecting the central skull base: CT and MR imaging. AJR Am J Roentgenol. 1992; 159:581–589. [PubMed: 1503031]
18. Gizewski ER, Maderwald S, Linn J, Dassinger B, Bochmann K, Forsting M, et al. High-resolution anatomy of the human brain stem using 7-T MRI. improved detection of inner structures and nerves? Neuroradiology. 2014; 56:177–186. [PubMed: 24357075]
19. Grams AE, Kraff O, Kalkmann J, Orzada S, Maderwald S, Ladd ME, et al. Magnetic resonance imaging of cranial nerves at 7 Tesla. Clin Neuroradiol. 2013; 23:17–23. [PubMed: 23015059]
20. Gu Y, Zhang X, Hu F, Yu Y, Xie T, Sun C, et al. Suprachiasmatic translamina terminalis corridor used in endoscopic endonasal approach for resecting third ventricular craniopharyngioma. J Neurosurg. 2015; 122:1166–1172. [PubMed: 25723303]
21. Hatipoglu HG, Cetin MA, Selvi A, Yuksel E. Role of magnetic resonance imaging in evaluating sphenoid sinus and internal carotid artery. J Laryngol Otol. 2009; 123:1331–1337. [PubMed: 19775490]
22. Juraschka K, Khan OH, Godoy BL, Monsalves E, Kilian A, Krischek B, et al. Endoscopic endonasal transsphenoidal approach to large and giant pituitary adenomas: institutional experience and predictors of extent of resection. J Neurosurg. 2014; 121:75–83.
23. Kang CK, Park CW, Han JY, Kim SH, Park CA, Kim KN, et al. Imaging and analysis of lenticulostriate arteries using 7.0-Tesla magnetic resonance angiography. Magn Reson Med. 2009; 61:136–144. [PubMed: 19097221]
24. Knosp E, Steiner E, Kitz K, Matula C. Pituitary adenomas with invasion of the cavernous sinus space: a magnetic resonance imaging classification compared with surgical findings. Neurosurgery. 1993; 33:610–617. discussion 617–618. [PubMed: 8232800]

25. Koutourousiou M, Fernandez-Miranda JC, Stefko ST, Wang EW, Snyderman CH, Gardner PA. Endoscopic endonasal surgery for suprasellar meningiomas: experience with 75 patients. J Neurosurg. 2014; 120:1326–1339. [PubMed: 24678782]
26. Kraff O, Fischer A, Nagel AM, Monninghoff C, Ladd ME. MRI at 7 Tesla and above: demonstrated and potential capabilities. J Magn Reson Imaging. 2015; 41:13–33. [PubMed: 24478137]
27. Laufer I, Anand VK, Schwartz TH. Endoscopic, endonasal extended transsphenoidal, transplanum transtuberculum approach for resection of suprasellar lesions. J Neurosurg. 2007; 106:400–406. [PubMed: 17367062]
28. Linn J, Peters F, Lummel N, Schankin C, Rachinger W, Brueckmann H, et al. Detailed imaging of the normal anatomy and pathologic conditions of the cavernous region at 3 Tesla using a contrast-enhanced MR angiography. Neuroradiology. 2011; 53:947–954. [PubMed: 21271242]
29. Magro E, Graillon T, Lassave J, Castinetti F, Boissonneau S, Tabouret E, et al. Complications Related to the Endoscopic Endonasal Transsphenoidal Approach for Nonfunctioning Pituitary Macroadenomas in 300 Consecutive Patients. World Neurosurg. 2016; 89:442–453. [PubMed: 26902781]
30. Marques JP, Kober T, Krueger G, van der Zwaag W, Van de Moortele PF, Gruetter R. MP2RAGE, a self bias-field corrected sequence for improved segmentation and T1-mapping at high field. Neuroimage. 2010; 49:1271–1281. [PubMed: 19819338]
31. Micko AS, Wohrer A, Wolfsberger S, Knosp E. Invasion of the cavernous sinus space in pituitary adenomas: endoscopic verification and its correlation with an MRI-based classification. J Neurosurg. 2015; 122:803–811. [PubMed: 25658782]
32. Moussazadeh N, Kulwin C, Anand VK, Ting JY, Gamss C, Iorgulescu JB, et al. Endoscopic endonasal resection of skull base chondrosarcomas: technique and early results. J Neurosurg. 2015; 122:735–742. [PubMed: 25594323]
33. Ostrom QT, Gittleman H, Fulop J, Liu M, Blanda R, Kromer C, et al. CBTRUS Statistical Report: Primary Brain and Central Nervous System Tumors Diagnosed in the United States in 2008–2012. Neuro Oncol. 2015; 17(Suppl 4):iv1–iv62. [PubMed: 26511214]
34. P. PFaB. Improved signal uniformity for balanced steady-state free precession by employing Direct Signal Control parallel transmission. Annual Meeting of the ISMRM. 2017:385.
35. Paek SL, Chung YS, Paek SH, Hwang JH, Sohn CH, Choi SH, et al. Early experience of pre- and post-contrast 7.0T MRI in brain tumors. J Korean Med Sci. 2013; 28:1362–1372. [PubMed: 24015044]
36. Pierallini A, Caramia F, Falcone C, Tinelli E, Paonessa A, Ciddio AB, et al. Pituitary macroadenomas: preoperative evaluation of consistency with diffusion-weighted MR imaging--initial experience. Radiology. 2006; 239:223–231. [PubMed: 16452397]
37. Pinker K, Ba-Ssalamah A, Wolfsberger S, Mlynarik V, Knosp E, Trattnig S. The value of high-field MRI (3T) in the assessment of sellar lesions. Eur J Radiol. 2005; 54:327–334. [PubMed: 15899332]
38. Pohmann R, Speck O, Scheffler K. Signal-to-noise ratio and MR tissue parameters in human brain imaging at 3, 7, and 9.4 tesla using current receive coil arrays. Magn Reson Med. 2016; 75:801–809. [PubMed: 25820458]
39. Ribas GC, Rodrigues AJ. The suprapetrosal craniotomy. J Neurosurg. 2007; 106:449–454. [PubMed: 17367068]
40. Shanno G, Maus M, Bilyk J, Schwartz S, Savino P, Simeone F, et al. Image-guided transorbital roof craniotomy via a suprabrow approach: a surgical series of 72 patients. Neurosurgery. 2001; 48:559–567. discussion 567–558. [PubMed: 11270546]
41. Song SW, Son YD, Cho ZH, Paek SH. Experience with 7.0 T MRI in Patients with Supratentorial Meningiomas. J Korean Neurosurg Soc. 2016; 59:405–409. [PubMed: 27446524]
42. Stamm AC, Wright CL, Knopp MV, Schmalbrock P, Heverhagen JT. Phase contrast and time-of-flight magnetic resonance angiography of the intracerebral arteries at 1.5, 3 and 7 T. Magn Reson Imaging. 2013; 31:545–549. [PubMed: 23219250]

43. Tabaee A, Anand VK, Barron Y, Hiltzik DH, Brown SM, Kacker A, et al. Endoscopic pituitary surgery: a systematic review and meta-analysis. J Neurosurg. 2009; 111:545–554. [PubMed: 19199461]

44. von Morze C, Xu D, Purcell DD, Hess CP, Mukherjee P, Saloner D, et al. Intracranial time-of-flight MR angiography at 7T with comparison to 3T. J Magn Reson Imaging. 2007; 26:900–904. [PubMed: 17896360]

45. Wolfsberger S, Ba-Ssalamah A, Pinker K, Mlynarik V, Czech T, Knosp E, et al. Application of three-tesla magnetic resonance imaging for diagnosis and surgery of sellar lesions. J Neurosurg. 2004; 100:278–286. [PubMed: 15086236]

46. Yagi A, Sato N, Takahashi A, Morita H, Amanuma M, Endo K, et al. Added value of contrast-enhanced CISS imaging in relation to conventional MR images for the evaluation of intracavernous cranial nerve lesions. Neuroradiology. 2010; 52:1101–1109. [PubMed: 20383633]

47. Yagi A, Sato N, Taketomi A, Nakajima T, Morita H, Koyama Y, et al. Normal cranial nerves in the cavernous sinuses: contrast-enhanced three-dimensional constructive interference in the steady state MR imaging. AJNR Am J Neuroradiol. 2005; 26:946–950. [PubMed: 15814950]

48. Zeineh MM, Parekh MB, Zaharchuk G, Su JH, Rosenberg J, Fischbein NJ, et al. Ultrahigh-resolution imaging of the human brain with phase-cycled balanced steady-state free precession at 7 T. Invest Radiol. 2014; 49:278–289. [PubMed: 24473366]

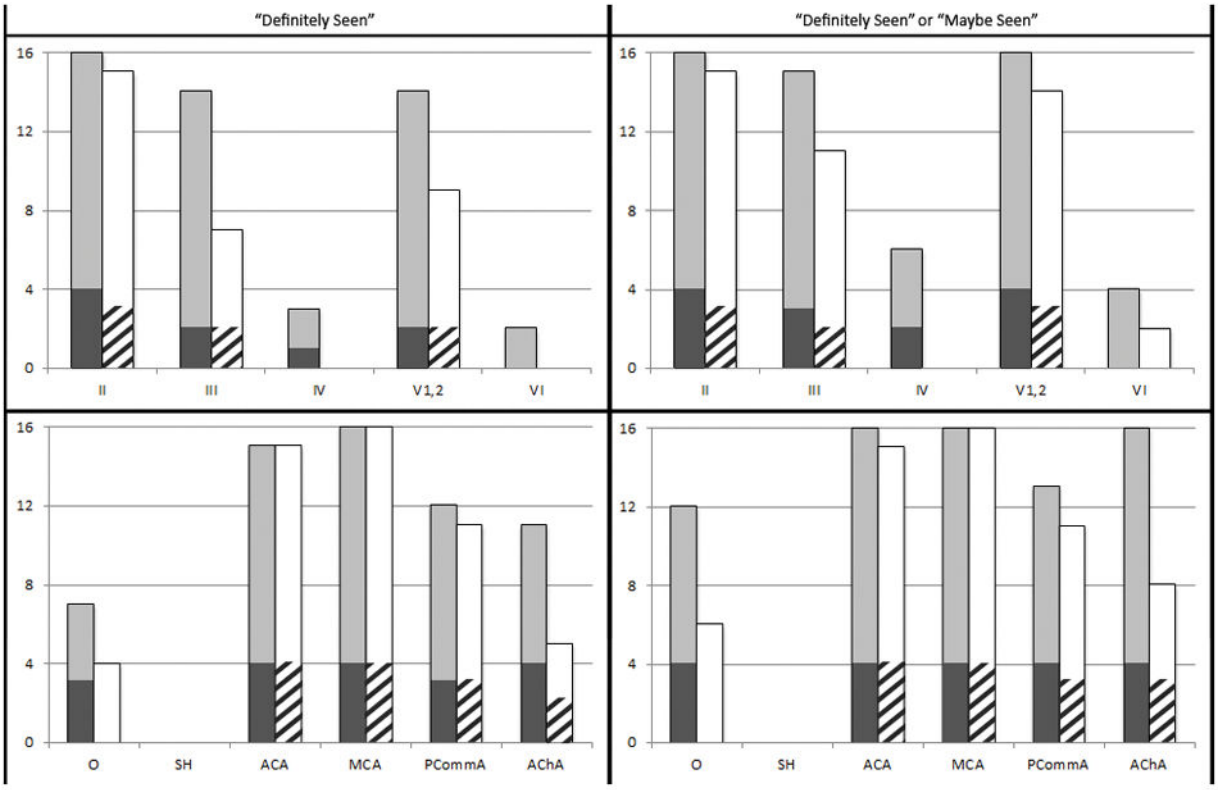

Figure 1. Detection rates of cranial nerves and ICA branches

The top row displays detection rates of cranial nerves II–VI and the bottom row displays detection rates of ICA branches. Light gray bars represent 7T results in patients with 1.5T scans available for comparison. Dark gray bars represent 7T results in patients with 3T scans available for comparison. White bars represent 1.5T results and striped bars represent 3T results.

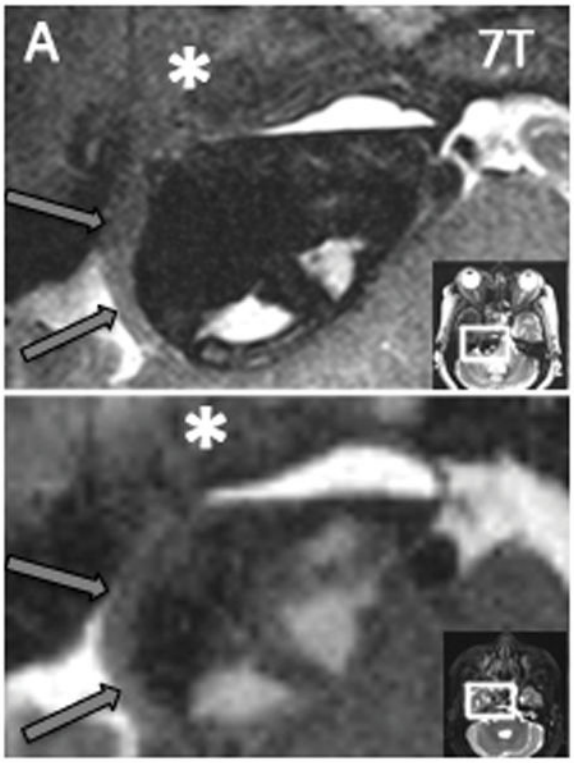

Figure 2. Tumor-trigeminal delineation at 3T and 7T

Axial T2W images of same patient at both 3T and 7T. The right trigeminal nerve (black arrow) is shown smoothly draped along the surface of the tumor, and distinction of nerve from tumor is easily made at 7T. At 3T, both the nerve and its border with the tumor are more difficult to resolve. The tumor margin is clearly delineated as it displaces the pons (P) with 7T, while the boundaries are blurred at 3T. A distinct fluid level (short white arrow) can be appreciated with 7T as well. Additionally, the fascicles of the left trigeminal nerve (long white arrow) are clearly defined as they approach Meckel's cave with 7T and are less clearly resolved with 3T.

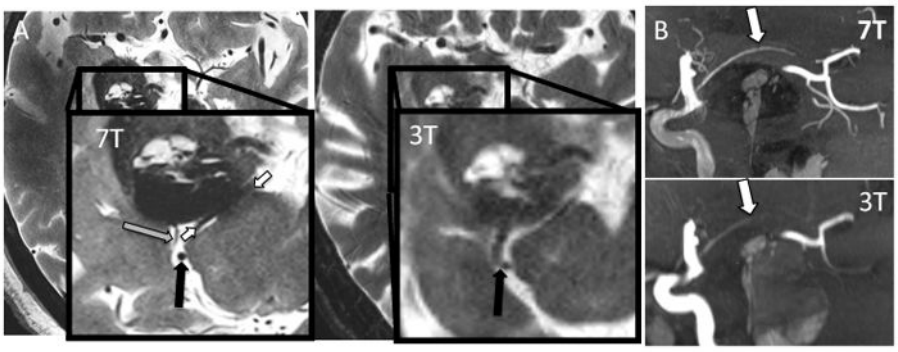

Figure 3. ICA branch detection at 3T and 7T

Sagittal Maximal Intensity Projection (MIP) of TOF MRA at both 3T and 7T. MRA acquisitions were fused to ensure identical tissue coverage. Imaging at 7T nicely shows the AChA (white) splayed over the tumor, while at 3T it is poorly seen over a shorter length. Additionally, other small vessels such as PCA tributaries projecting inferiorly are well visualized at 7T but not visualized at 3T.

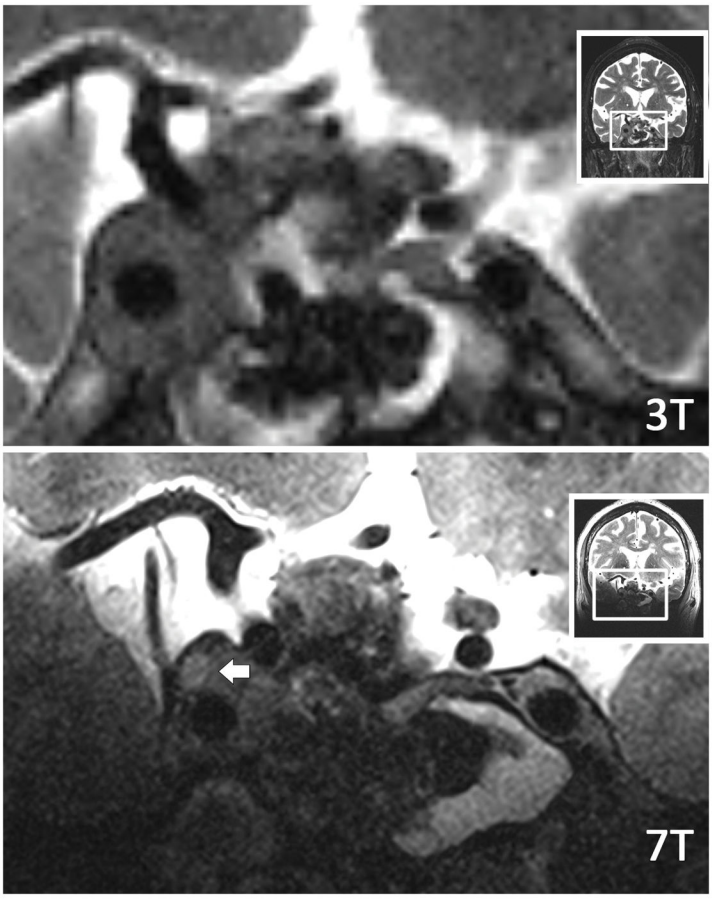

Figure 4. Characterization of a macroadenoma within the right cavernous sinus and mass effect of tumor on adjacent cranial nerves

Two corresponding coronal T2W TSE images at 3T and 7T acquired per research protocol in same subject. A and B are in the same plane in the interpeduncular cistern at 3T and 7T, respectively, while C and D section more anteriorly through the cavernous sinuses. (A and B) At 7T, the left oculomotor (large black arrow), trochlear (small black arrow), and trigeminal nerve (small white arrow) can be seen approaching the cavernous sinus. At 3T, the oculomotor and trigeminal nerves are less clearly defined, and the trochlear nerve is not visible. The large macroadenoma clearly displaces the right oculomotor nerve superiorly (large white arrow) at 7T, while at 3T the nerve is not as well resolved. (C and D) At 7T, this nerve can be traced as it is courses around the large mass and eventually seen as a region of higher intensity in the cavernous sinus. At 3T, the course of the nerve is lost amid tumor signal.

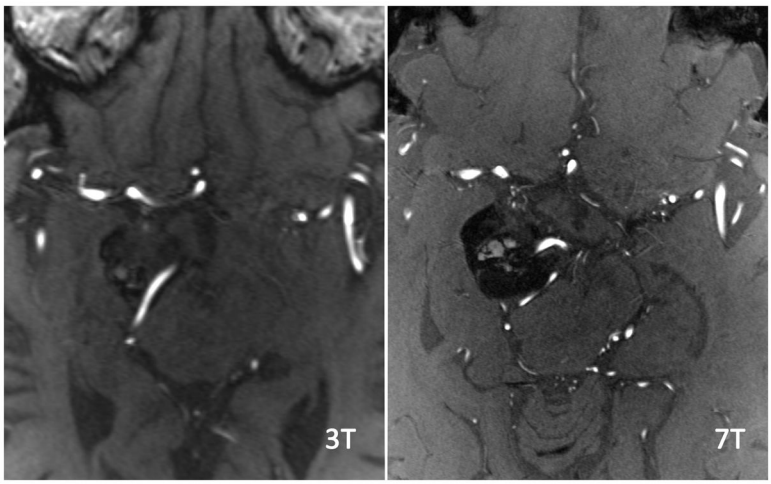

Figure 5. Vessels feeding tumor

As in Figure 3, these images were acquired using TOF MRA per our research protocol at both 3T and 7T in the same patient. The slice angle is slightly different, and the slices were chosen based on the optimal slice at 3T to view the small feeding arteries. A comparable slice at 7T was then found. Small vessels feeding the tumor (white arrow) can be resolved at 7T that cannot be appreciated with 3T. Additionally, small perforating branches from the ACA and MCA territories can be appreciated throughout the 7T image.

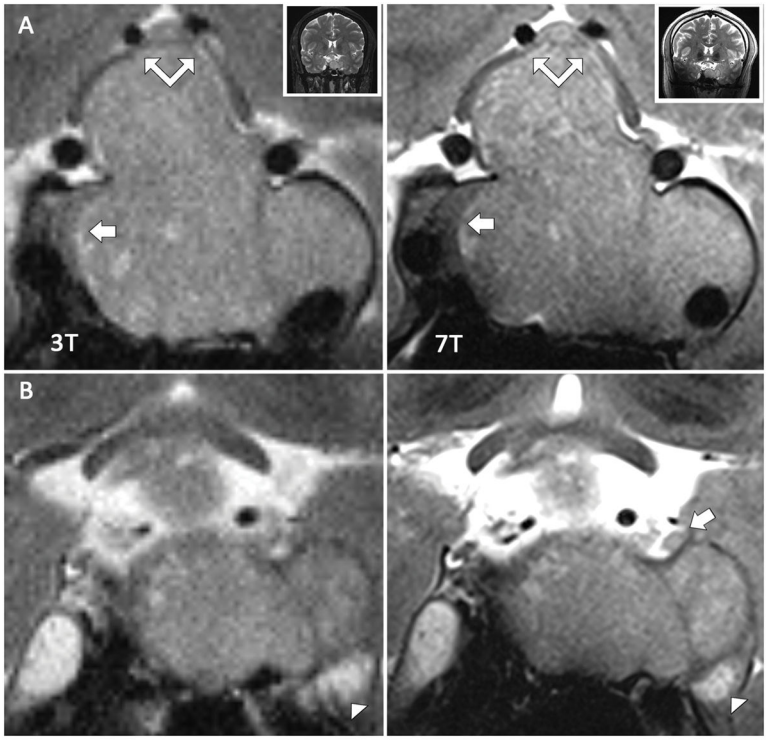

Figure 6. Coronal Images of Pituitary Adenoma and Cavernous Structures

Coronal T2W TSE images from same patient acquired with both 3T and 7T research protocols. A and B are similar slices obtained through the cavernous sinus at 3T and 7T respectively. C and D are similar slices obtained slightly posterior to A and B. (A and B) At both 3T and 7T, a large isointense pituitary adenoma is appreciated with good delineation of the hypointense normal gland on the right. With 7T, however, the right medial wall of the cavernous sinus (short white arrow) is seen to be intact while with 3T it is unclear if the wall has been infiltrated. Additionally, the chiasm can be seen draped over the tumor at both field strengths (double arrow), but is better resolved at 7T. (C and D) At 7T, the left third nerve (white arrow) is appreciated being displaced superiorly by the invasive mass. At 3T, the nerve cannot be visualized. Additionally, the fascicles of the trigeminal nerve are better resolved in Meckel's cave at 7T MRI (long white arrow).

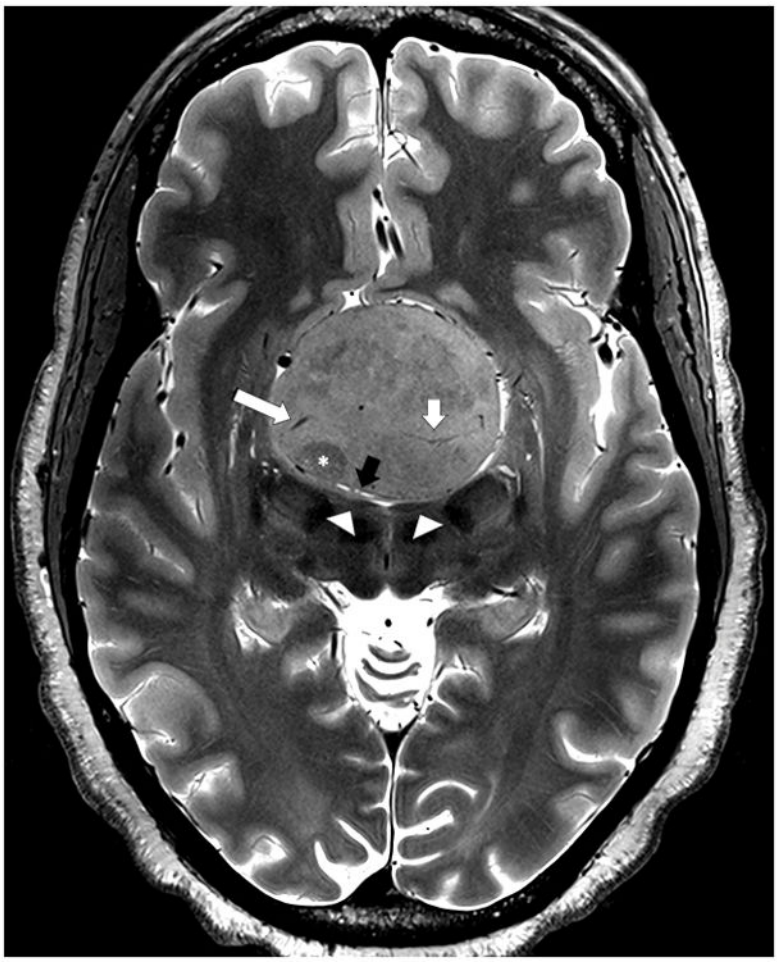

Figure 7. 7T images of giant macroadenoma

Axial T2-weighted TSE image obtained at 7T in a patient with a giant pituitary adenoma. The image shows tumor heterogeneity including zone of lower signal suggesting a region of firmer tumor (asterisk), venous drainage (long white arrow), tumor arterial supply (short white arrow) and compressed adjacent anatomy including flattened mammillary bodies (arrowheads) and the lamina terminalis (black arrow).

Table 1

Protocol for scans performed with 7T.

Parameters	T1-W MP2-RAGE	T2 TSE	TOF Angiography
TE/TR (ms)	5.06/10.4/6000	59/6000	5.6/18
TI (ms)	1050–3000	-	-
Resolution (mm)	0.79 × 0.79 × 0.79	0.39 × 0.39 × 2.0	0.35 × 0.26 × 0.40
Number of slices	208	55	240 (4 slabs)
Flip Angle (°)	4–5	140	20
Slab thickness (mm)	164		24
Bandwidth (Hz/pixel)	130	279	121
Parallel MRI Factor	2	2	2
Field of View (mm)	224 × 178	200 × 170	200 × 170
Acquisition Plane	AC-PC	AC-PC	Axial oblique
Acquisition Time (min)	6:35	6:13	10:13

Table 2

Protocol for scans performed with 3T.

Parameters	T1-W MP-RAGE	T2 TSE	TOF Angiography
TE/TR (ms)	2.07/2400	83/8163	7.2/27
TI (ms)	1000	N/A	N/A
Resolution (mm)	0.8x0.8x0.8	0.25x0.27x2.0	0.49x0.49x0.7
Number of slices	224	68	115
Flip Angle (°)	8	123	25
Slab thickness (mm)	179	136	80.5
Bandwidth (Hz/pixel)	240	360	100
Parallel MRI Factor	2	2	2
Field of View (mm)	256x256	219x219	224x168
Acquisition Plane	Sagittal	Tra/Sag	Tra
Acquisition Time (min)	4:12	6:42	4:17

Table 3

Tumor characteristics seen with each field strength. Delineation of the chiasm and tumor neovasculature were seen with more confidence at 7T. It must be stated, however, that not all pathologies will have each of these features. Rates of detection by imaging can only be confirmed with intraoperative findings.

Field	Optic chiasm compression		Cystic/Hemorrhagic Component		Tumor vasculature	
	2	2+1	2	2+1	2	2+1
7T	8/8	8/8	3/8	3/8	3/8	5/8
3T+1.5T	5/8	6/8	3/8	4/8	1/8	4/8

Table 4

Technical artifacts. This table shows the frequency with which each technical artifact was seen with each field strength. Of note, B_1 artifacts were seen in 4/10 instances, while these artifacts were not seen at all at either 3T or 1.5 T. This is due to the shortened waveform of the transmit field with 7T MRI.

	Artifact	1 - Negligible	2 - Minimal	3 - Moderate	4 - High	5 - Severe
7T	Motion	3/10	2/10	3/10	2/10	0/10
	B_0	0/10	6/10	4/10	0/10	0/10
	B_1	0/10	3/10	2/10	4/10	1/10
3T	Motion	0/2	0/2	2/2	0/2	0/2
	B_0	1/2	1/2	0/2	0/2	0/2
	B_1	2/2	0/2	0/2	0/2	0/2
1.5	Motion	4/7	2/7	1/7	0/7	0/7
	B_0	5/7	2/7	0/7	0/7	0/7
	B_1	7/7	0/7	0/7	0/7	0/7